



Magnetic ordering in the layered oxyhalide $\text{Sr}_2\text{NiO}_2\text{Cl}_2$

Robert D. Smyth^a, Dmitry Khalyavin^b, Yoshihiro Tsujimoto^c, Kazunari Yamaura^c,
Simon J. Clarke^{a,*}

^a Department of Chemistry, University of Oxford, Inorganic Chemistry Laboratory, South Parks Road, Oxford, OX1 3QR, UK

^b ISIS Facility, Rutherford Appleton Laboratory, Harwell Oxford, Didcot, OX1 10QX, UK

^c Research Centre for Materials Nanoarchitectonics (MANA), National Institute for Materials Science (NIMS), 1-1 Namiki, Tsukuba, Ibaraki, 305-0044, Japan

ARTICLE INFO

Keywords:

Oxyhalide
Oxychloride
Magnetic ordering
Antiferromagnetic
High pressure

ABSTRACT

The full characterisation of the high-pressure-synthesised, metastable layered oxyhalide $\text{Sr}_2\text{NiO}_2\text{Cl}_2$ is reported. It is comprised of infinite NiO_2 layers along with double rock salt Sr_2Cl_2 layers and is closely related to the $n = 1$ Ruddlesden-Popper phases. At ambient temperature, it crystallises in the tetragonal space group $I4/mmm$ with 2 formula units per unit cell with the basal lattice parameters $a = b = 4.03417(2)$ Å and the stacking direction lattice parameter, $c = 15.1058(1)$ Å. A tiny cusp in the temperature dependence of the magnetic susceptibility in a previous report suggested that this oxyhalide underwent long-range magnetic order and therefore contained high-spin Ni^{2+} ions. Powder neutron diffraction has confirmed that $\text{Sr}_2\text{NiO}_2\text{Cl}_2$ is a localised-moment oxyhalide, adopting the high-spin $S = 1$ configuration with fully occupied d_{xz} , d_{yz} and d_{xy} orbitals and partially occupied d_{z^2} and $d_{x^2-y^2}$ orbitals. The Ni^{2+} magnetic moments order antiferromagnetically below ≈ 180 K in a G-type arrangement on a $\sqrt{2}a \times \sqrt{2}a \times c$ expansion of the nuclear cell with the propagation vector $(\frac{1}{2}, \frac{1}{2}, 0)$ and with a saturated long-range ordered magnetic moment of $1.57(7)$ μ_B per Ni^{2+} cation which is in line with previously calculated computational results and showing that the ligand field around the Ni^{2+} cation is not sufficiently anisotropic to drive it into the low-spin, diamagnetic configuration found for this d^8 cation in square planar or highly elongated octahedral coordination.

1. Introduction

Mixed-anion solids, for which there are now several reviews [1–4] are an under-explored class of material. The introduction of multiple anions enables control of band gaps and transition metal coordination environments and increases the range of materials properties. For example, the oxychalcogenide BiCuOSe is currently the best p -type thermoelectric material that is free of lead or tellurium [5], oxypnictides such as F-doped LaFeAsO are a new class of high-temperature superconductor [6], oxynitrides such as $\text{Ta}_{3-x}\text{Zr}_x\text{O}_x\text{N}_{5-x}$ which has use as an inert inorganic pigment may help with the transition away from pigments containing toxic metals such as antimony and arsenic [7]. Oxyhalides such as $\text{Sr}_2\text{CuO}_2\text{Cl}_2$ offer a highly anisotropic coordination environment for first row transition metal ions and this compound is an ideal 2D quantum Heisenberg antiferromagnet [8] and also a “parent” compound of a host of high-temperature cuprate superconductors.

In mixed-anion compounds, it is extremely common to find anion segregation between oxide and the larger more polarisable pnictide,

chalcogenide or halide anions (except normally for N^{3-} or F^-) which results in layered structures with each anion occupying a different layer and sometimes dictating the structural ordering of cations through chemical preferences. The properties can then sometimes be exploited through topotactic reactions [9–11] or by tuning the ligand field around the central cation [12].

Tsujimoto et al. previously reported the synthesis of the novel oxyhalide $\text{Sr}_2\text{NiO}_2\text{Cl}_2$, obtained via a high pressure synthesis [13]. The compound is isostructural with $\text{Sr}_2\text{CuO}_2\text{Cl}_2$ and $\text{Sr}_2\text{CoO}_2\text{Cl}_2$ (which are accessible in ambient pressure syntheses) and crystallises in the $I4/mmm$ space group and can be envisaged as infinite NiO_2 layers along with double-rock-salt Sr_2Cl_2 layers (see Fig. 1) with the Ni–Cl bonds calculated to contribute between them just 16.8% to the total bond valence sum which means the Ni^{2+} centres can be described as being in highly elongated octahedra or pseudo square-planar NiO_4 units. Tsujimoto et al. noted a cusp in the magnetic susceptibility suggestive of a magnetic ordering transition indicative that Ni^{2+} was in the high-spin, $S = 1$ state rather than low spin and diamagnetic [13]. Furthermore, Zhou et al.

* Corresponding author.

E-mail address: simon.clarke@chem.ox.ac.uk (S.J. Clarke).

<https://doi.org/10.1016/j.solidstatesciences.2023.107297>

Received 8 June 2023; Received in revised form 22 August 2023; Accepted 27 August 2023

Available online 28 August 2023

1293-2558/© 2023 The Authors. Published by Elsevier Masson SAS. This is an open access article under the CC BY license (<http://creativecommons.org/licenses/by/4.0/>).

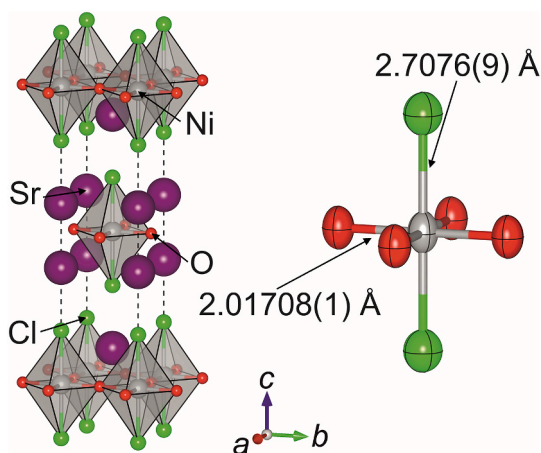


Fig. 1. Crystal structure of $\text{Sr}_2\text{NiO}_2\text{Cl}_2$ [18]. Anisotropic displacement parameters from powder neutron diffraction data are shown at 99% probability.

performed a systematic theoretical study on $\text{Sr}_2\text{NiO}_2\text{Cl}_2$ and came to the conclusion that the unusual coordination environment plays a crucial role in the magnetic and electronic properties of $\text{Sr}_2\text{NiO}_2\text{Cl}_2$ and predicted G-type, antiferromagnetic ordering [14].

To complete the characterisation of this metastable phase, it was clear that powder neutron diffraction was the key to elucidating the magnetic structure of $\text{Sr}_2\text{NiO}_2\text{Cl}_2$. Here, we report the high-pressure synthesis on a multi-gram scale of a sample of this compound with a high level of purity and report the experimental magnetic structure of $\text{Sr}_2\text{NiO}_2\text{Cl}_2$ for comparison with related compounds and recent theoretical calculations.

2. Experimental section

2.1. Synthesis

The sample of $\text{Sr}_2\text{NiO}_2\text{Cl}_2$ used for the analysis in this paper was synthesised in a refinement of the method reported by Tsujimoto et al. in the communication reporting the discovery of this phase [13]. It was found that using NiO as a nickel source yielded a much purer product than when elemental nickel powder was used (see Fig S1).

Equimolar amounts of in-house synthesised SrO (from the thermal decomposition of SrCO_3 (Rare Metallic Co., Ltd, 99.9%) at 1300 °C in a flowing O_2 atmosphere), NiO (Kojundo Chemical Laboratory Co., Ltd, 99.9%) and SrCl_2 (Rare Metallic Co., Ltd, 99.9%), both of which were stored in an Ar-filled glovebox immediately after receiving them, were thoroughly mixed together and formed into 2×0.4 g (0.8 g per reaction) pellets enclosed within a Pt capsule. This capsule was then loaded into a belt-type, high-pressure apparatus with an applied pressure of 3 GPa and heated at 1400 or 1500 °C for a dwell time of 1 h. The sample was then subsequently quenched rapidly to room temperature with a slow release of pressure, yielding a dark green solid. The 1.6 g sample that was used for PND was a mixture of the batches prepared at 1400 and 1500 °C (2×0.8 g batches).

2.2. Powder X-ray diffraction (PXRD)

The reaction progression was monitored in house using a Rigaku MiniFlex-600 diffractometer with a mixture of both $\text{CuK}_{\alpha 1}$ and $\text{CuK}_{\alpha 2}$ radiation. Due to the air and moisture sensitivity of the samples, the portions extracted for the X-ray measurements were covered in paraffin oil prior to measurement to avoid degradation of the sample and then discarded.

Synchrotron powder X-ray diffraction (SPXRD) for detailed structural analysis using higher resolution, higher intensity and higher-Q powder data was previously performed on a sample prepared from Ni

powder on the X-ray detector installed on BL15XU, the NIMS beamline at Spring-8, [13,15] (with comparison between the samples shown in Table S1) further analysis of the purer sample prepared from NiO and used for the PND measurements was performed using the I11 beamline at the Diamond Light Source [16], UK with radiation of wavelength $\lambda = 0.824385(10)$ Å (calibrated before the session using a silicon standard). To prepare for these measurements, the sample was ground thoroughly in a 1:1 mixture with ground silica glass (which reduces X-ray absorption and preferred orientation effects) and flame-sealed under argon in a 0.5 mm borosilicate capillary.

For measurements over a range of temperatures, a position-sensitive detector (Mythen PSD) was used which is optimised for rapid data collection and allowed for scans at 1 °C intervals between 300 K and 100 K with cooling provided by an Oxford Cryosystems cryostream.

2.3. Powder neutron diffraction (PND)

Powder neutron diffraction (PND) was used to probe changes in the crystal structure as a function of temperature and to characterise the long-range magnetic ordering proposed by the computation of Zhou et al. [14] as well as previous magnetometry performed by Tsujimoto et al. [13].

The 1.6 g sample of $\text{Sr}_2\text{NiO}_2\text{Cl}_2$ prepared using NiO was loaded into a 6 mm vanadium can and sealed with indium wire and measured on the time-of-flight (ToF) diffractometer WISH at the ISIS facility, UK [17]. This instrument is optimised for high count-rates and high resolution at long d -spacing where magnetic Bragg scattering is most prevalent and produces high-resolution data at sufficiently low d -spacings to adequately describe the nuclear structure. An Oxford blue cryostat was used to cool the sample.

2.4. Magnetometry

The magnetic susceptibility of $\text{Sr}_2\text{NiO}_2\text{Cl}_2$ was measured using a Quantum Design MPMS-3 SQUID magnetometer. Approximately 30 mg of powder was contained within a gelatin capsule to perform the measurement. The temperature dependence was measured in the range $2 \leq T(\text{K}) \leq 330$. During these measurements, the sample was first cooled in the absence of a magnetic field (zero-field cooled (ZFC)) prior to measurement in an applied field of 1000 Oe, with a second measurement performed after cooling in the measuring field (field-cooled (FC)). The magnetisation isotherm was also measured in the range $-7 \leq H(\text{T}) \leq 7$ with cooling in a 7 T field to 5 K before measurement.

3. Results and discussion

3.1. Crystal structure

A high purity phase of $\text{Sr}_2\text{NiO}_2\text{Cl}_2$ as determined by laboratory PXRD and consistent with previously reported patterns [13] was used for detailed structural characterisation using synchrotron PXRD and PND measurements. The Rietveld refinements against both sets of data at ambient temperature are shown in Fig. 2 with further plots shown in Figs S2 – S5.

Rietveld refinement confirmed that $\text{Sr}_2\text{NiO}_2\text{Cl}_2$ crystallises in the tetragonal $I4/mmm$ space group with similar lattice parameters to those previously reported [13]. The extracted structural parameters obtained from SPXRD and PND are displayed in Table 1 below. Variable temperature PXRD did not suggest any lowering of symmetry or discontinuities of the lattice parameters but did show a small downturn in the change in the a lattice parameter and hence the Ni–O distance ($= a/2$) coinciding with the magnetic ordering temperature which is most likely magnetostrictive in origin (see Fig. 3 as well as supporting information Figs S6 and S7 for local coordination plots). The behaviour of the normalised lattice parameters is typical of that of layered materials whereby they are much less compressible within the basal plane within which the

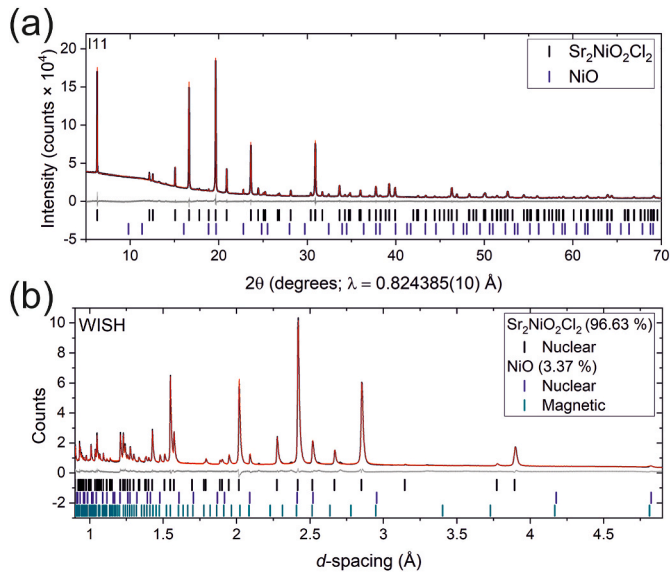


Fig. 2. (a) Room temperature Rietveld refinement of $\text{Sr}_2\text{NiO}_2\text{Cl}_2$ against SPXRD. $R_{wp} = 2.283\%$; $\chi^2 = 2.500$ and (b) Rietveld refinement of $\text{Sr}_2\text{NiO}_2\text{Cl}_2$ against bank 5/6 of the WISH diffractometer at ISIS. $R_{wp} = 1.989\%$; $\chi^2 = 0.023$.

Table 1

Structural Rietveld refinement against SPXRD and PND data for $\text{Sr}_2\text{NiO}_2\text{Cl}_2$ at room temperature.

Radiation	SPXRD	PND
a (Å)	4.02967(1)	4.03417(2)
c (Å)	15.09577(9)	15.1058(1)
v (Å ³)	245.129(2)	245.841(3)
$z(\text{Sr})^a$	0.39248(3)	0.39255(8)
$z(\text{Cl})^a$	0.17887(7)	0.17907(6)
$U_{11}(\text{Sr})$ (Å ²)	0.0042(5)	0.0159(4)
$U_{33}(\text{Sr})$ (Å ²)	0.0130(4)	0.0155(8)
$U_{11}(\text{Ni})$ (Å ²)	0.0031(4)	0.0109(4)
$U_{33}(\text{Ni})$ (Å ²)	0.0146(6)	0.0203(7)
$U_{11}(\text{O})$ (Å ²)	0.003(2)	0.0126(5)
$U_{22}(\text{O})$ (Å ²)	0.000(1)	0.0117(6)
$U_{33}(\text{O})$ (Å ²)	0.025(2)	0.0215(6)
$U_{11}(\text{Cl})$ (Å ²)	0.0116(4)	0.0177(3)
$U_{33}(\text{Cl})$ (Å ²)	0.0123(8)	0.0212(7)

^a Sr, 4e(0,0,z); Ni, 2a(0,0,0); O, 4c(0, 1/2,0); Cl, 4e(0,0,z).

rigid NiO_2 sub-lattice is orientated.

$\text{Sr}_2\text{NiO}_2\text{Cl}_2$ is isostructural with other oxyhalides prepared at ambient or high pressures, and is an anion-ordered variant of the $n = 1$ Ruddlesden-Popper series of compounds with the K_2NiF_4 structure. It also has a similar structural framework to a series of oxide chalcogenides, exemplified by the recently reported $\text{Sr}_2\text{NiO}_2\text{Cu}_2\text{Ch}_2$ ($\text{Ch} = \text{S}, \text{Se}$) [12]. The refined structural parameters are compared in Table 2 with comparison to closely related oxyhalide analogues displayed in Table S2. Formally the oxychalcogenides $\text{Sr}_2\text{NiO}_2\text{Cu}_2\text{Ch}_2$ are related to the oxyhalides by the replacement of the halide by chalcogenide and balancing of the charge by incorporation of the Cu^+ coinage metal ion in the chalcogenide layers. The separation of the adjacent NiO_2 layers which are related by the body centring translations is smaller in the oxychloride because of the lack of an ion between adjacent layers of chloride ions. The lack of this ion competing for the halide results in a shorter Ni–Cl distance in $\text{Sr}_2\text{NiO}_2\text{Cl}_2$ than the Ni–Se distance in $\text{Sr}_2\text{NiO}_2\text{Cu}_2\text{Se}_2$, while the two have very similar Ni–O distances. This suggests a less anisotropic ligand field in $\text{Sr}_2\text{NiO}_2\text{Cl}_2$ than in $\text{Sr}_2\text{NiO}_2\text{Cu}_2\text{Se}_2$, and so the high-spin Ni^{2+} found in $\text{Sr}_2\text{NiO}_2\text{Cu}_2\text{Se}_2$ was also expected for $\text{Sr}_2\text{NiO}_2\text{Cl}_2$ as proposed in the computational study by Zhou et al. [14].

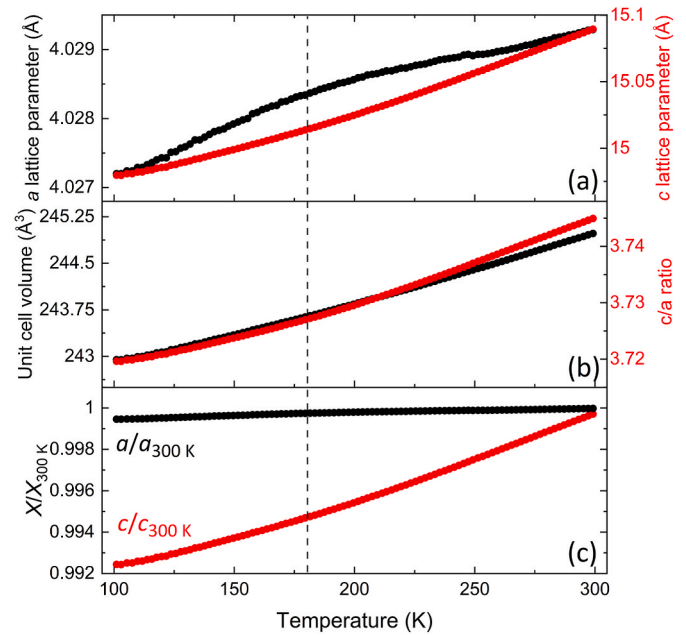


Fig. 3. (a) Refined lattice parameters of a and c for $\text{Sr}_2\text{NiO}_2\text{Cl}_2$ from I11 data, (b) unit cell volume and c/a ratio, (c) a and c values normalised to their values at 300 K. Error bars are within the plotted points, the dashed line is a guide to the eye around T_N .

Table 2

Comparison of lattice parameters and selected bond lengths of $\text{Sr}_2\text{NiO}_2\text{Cl}_2$ compared with $\text{Sr}_2\text{NiO}_2\text{Cu}_2\text{S}_2$ and $\text{Sr}_2\text{NiO}_2\text{Cu}_2\text{Se}_2$.

Compound	$\text{Sr}_2\text{NiO}_2\text{Cl}_2$	$\text{Sr}_2\text{NiO}_2\text{Cu}_2\text{S}_2$	$\text{Sr}_2\text{NiO}_2\text{Cu}_2\text{Se}_2$
Reference	This work	Ref. [1]	Ref. [12]
Radiation	PND	PND	PXRD/PND
a (Å)	4.03417(2)	3.92159(2)	4.026470(8)
c (Å)	15.1058(1)	18.11558(15)	18.40612(4)
c/a	3.74447(3)	4.61945(4)	4.57128(1)
Volume (Å ³)	245.841(3)	278.597(5)	298.408(1)
Ni–O (Å) [4]	2.01708(1)	1.96080(1)	2.013235(4)
Ni–X ^a (Å) [2]	2.7076(9)	3.1054(8)	3.0843(3)
Ni–X ^a /Ni–O	1.3423(5)	1.5837(4)	1.5320(1)

X^a = Cl, S or Se.

3.2. Magnetometry

Magnetometry measurements were qualitatively consistent with those previously reported [13]. $\text{Sr}_2\text{NiO}_2\text{Cl}_2$ exhibits a broad maximum similar to those commonly found in low-dimensional antiferromagnetic systems around 150–180 K which was tentatively identified as the Néel temperature (Fig. 4). The 5 K magnetisation isotherm shows displacement away from the origin, suggesting that there is a glassy component to the magnetism of the sample, and it is possible that this, together with the divergence of the zero-field-cooled and field-cooled curves is due to a miniscule amount of impurity which might also lead to the large up-turn in the susceptibility at low temperature. The difference in the susceptibility at room temperature compared to the previous report is likely down to the change in the Ni-source in the synthesis yielding a much purer product (see Fig S1.).

3.3. Magnetic ordering

The magnetic susceptibility data for this compound suggested that the onset of long-range magnetic order with a proposed Néel temperature (T_N) of approximately 160 K. To probe this further, low temperature PND was used. Ni^{2+} has a spin-only magnetic moment of $2 \mu_B$ and

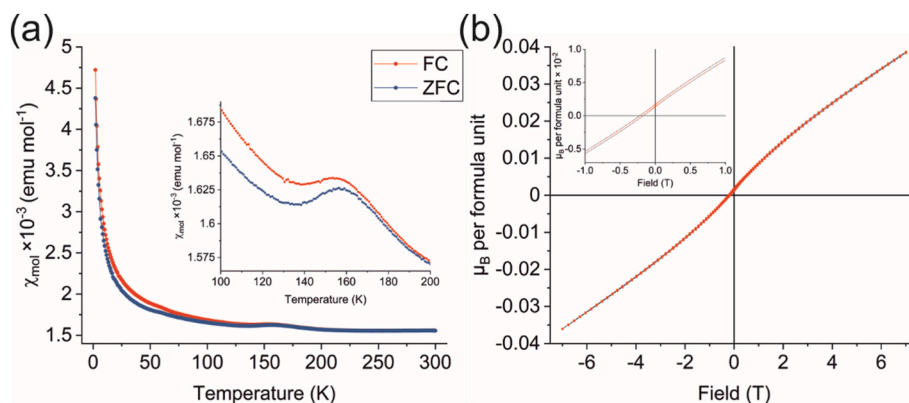


Fig. 4. (a) ZFC/FC plot of $\text{Sr}_2\text{NiO}_2\text{Cl}_2$ measured in an applied field of 1000 Oe. The inset zooms in on a kink identified as coinciding with the magnetic ordering temperature. (b) 5 K magnetisation isotherm emphasising the displacement from the origin in the inset.

therefore the magnitude of the magnetic scattering would be anticipated to be small. As such, WISH is the ideal instrument with its high signal-to-noise ratio in the region of the magnetic scattering meaning that small magnetic ordered moments of the order of $0.3 \mu_B$ or less are distinguishable from the background [19]. Rietveld refinement against the data at 1.5 K is shown in Fig. 5 and Figs S8–S11 with all data obtained on cooling shown in Fig S12.

The data had peaks at large d -spacing which were not accounted for by the nuclear model and grew in intensity on cooling as shown in Fig. 6 and annotated in Fig. 5 with asterisks, suggesting that they were magnetic in origin; also present is the characteristic (111) magnetic reflection from the small amount of NiO impurity denoted by a triangle in Fig. 5 [20].

The magnetic Bragg peaks were indexed on a propagation vector, $k = (\frac{1}{2} \frac{1}{2} 0)$ expansion of the nuclear cell and subsequent symmetry mode analysis was conducted using the ISODISTORT software [21]. The structure was analysed assuming $P1$ space group symmetry so that all possible modes could be considered. In conjunction with TOPAS V6, [22] it was determined that a singular magnetic symmetry mode did not yield a satisfactory fit to the data and so a combination of modes was investigated. It was found that a combination of the $\text{mX}2+$ and $\text{mX}3+$ modes gave a visually and statistically satisfactory fit during Rietveld refinement (fit shown in the inset of Fig. 5). Refining moments aligned along the ab -plane (i.e. just activating the $\text{mX}3+$ mode) resulted in an intensity mismatch for the (101) or (011) reflections at $\approx 5.33 \text{ \AA}$, where more than half of the intensity of the peak in this model was missing whereas moments aligned only along the c -axis (i.e. just activating the $\text{mX}2+$ mode) didn't give enough intensity to the (100) and (010) reflections at $\approx 5.71 \text{ \AA}$ as well as overestimating the (101) and (011) reflections. Admixture of these 2 magnetic modes allowed for much better statistical and visual agreement with the experimental results. Once the magnetic

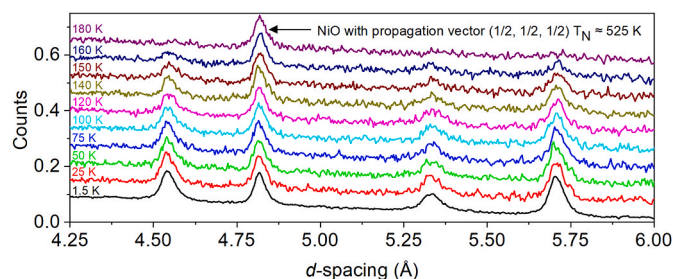


Fig. 6. Raw PND data for $\text{Sr}_2\text{NiO}_2\text{Cl}_2$ from the 2/9 bank of the WISH diffractometer.

symmetry modes were identified, ISODISTORT allowed for the determination of the magnetic space group symmetry. It was found that the $P6_3/bca$ magnetic space group (61.439 in the Belov, Neronova and Smirnova (BNS) scheme) or $C_{2v}m'ca'$ magnetic space group (64.16.543 in the Opechowski and Guccione (OG) scheme) [23] was the highest-symmetry magnetic space group that could account for the observed magnetic intensity from the PND data. This is a lowering in symmetry from the nuclear cell but no structural distortion is evident within the resolution of the powder data as shown in Fig S13.

This results in Ni^{2+} moments arranged antiferromagnetically in a G-type array as shown in Fig. 7. The refined Ni^{2+} moment had a magnitude of $1.57(7) \mu_B$ at 1.5 K ($\mu_a = \mu_b = 1.00(7) \mu_B$; $\mu_c = 1.22(6) \mu_B$). This is similar behaviour to the recently reported and closely related series of compounds $\text{Sr}_2\text{NiO}_2\text{Cu}_2(\text{Se}_{1-x}\text{S}_x)^{12}$ and also confirms the results from the computational study conducted by Zhou et al. [14] The reduction from the spin-only magnetic moment of $2 \mu_B$ can be attributed to a degree of

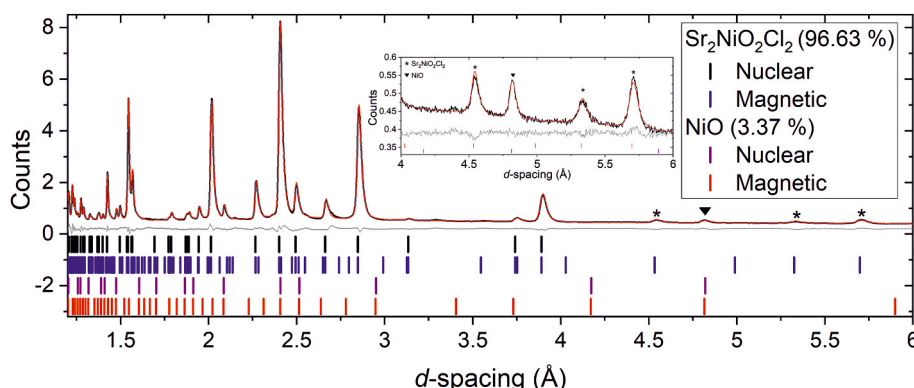


Fig. 5. Rietveld refinement at 1.5 K of $\text{Sr}_2\text{NiO}_2\text{Cl}_2$ against bank 2/9 of the WISH diffractometer at ISIS. $R_{wp} = 3.019\%$; $\chi^2 = 0.031$.

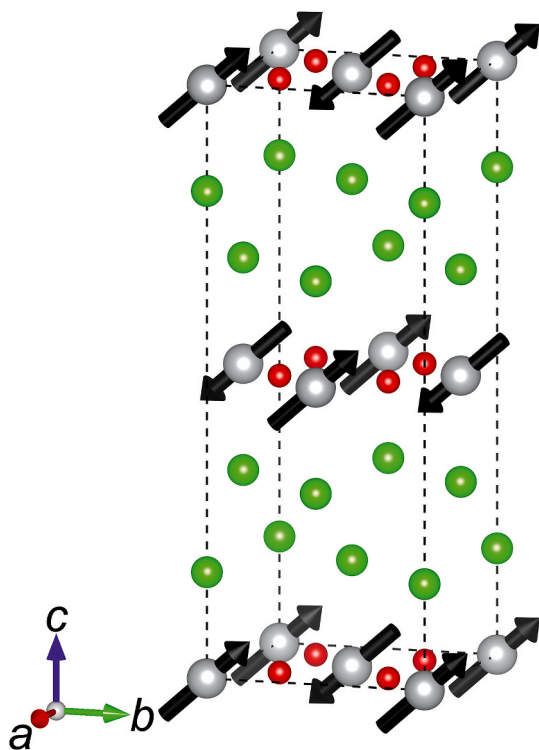


Fig. 7. The magnetic structure of $\text{Sr}_2\text{NiO}_2\text{Cl}_2$ with Ni^{2+} moments arranged in a G-type fashion with moments tilted between the ab -plane and the c -axis.

covalency in the bonding which is common for transition metal oxides and it is consistent with the calculated spin density of $1.6 \mu_B$ [14].

Fig. 8 shows the evolution of the Ni^{2+} moment on heating from the saturated value of $1.57(7) \mu_B$. From this, we infer that the Néel temperature (T_N) of this material can be extrapolated to ≈ 180 K where the long-range ordered moment develops. The drop in susceptibility below 150 K coincides approximately with the saturation of the long-range-ordered moment.

4. Conclusion

An adapted synthetic approach has enabled $\text{Sr}_2\text{NiO}_2\text{Cl}_2$ to be synthesised under high pressure on the bulk scale and with higher purity than previously reported [13]. Detailed analysis of the crystal structure and comparison with related materials $\text{Sr}_2\text{NiO}_2\text{Cu}_2\text{Se}_2$ and $\text{Sr}_2\text{NiO}_2\text{Cu}_2\text{S}_2$ show that when there is competition with Ni for the apical non-oxide anion the NiO_4X_2 octahedron is more elongated and the apical anion makes a smaller contribution to the Ni bond valence sum: chloride anions contribute a total of 16.8% to the total Ni BVS in $\text{Sr}_2\text{NiO}_2\text{Cl}_2$ while $\text{Sr}_2\text{NiO}_2\text{Cu}_2\text{Se}_2$ and $\text{Sr}_2\text{NiO}_2\text{Cu}_2\text{S}_2$ have a coordination closer to square planar with contributions of 9.33 and 6.05% respectively from selenide and sulfide anions. $\text{Sr}_2\text{NiO}_2\text{Cl}_2$ is thus firmly in the high-spin Ni^{2+} regime while high-spin $\text{Sr}_2\text{NiO}_2\text{Cu}_2\text{Se}_2$ and low-spin $\text{Sr}_2\text{NiO}_2\text{Cu}_2\text{S}_2$ straddle the high-spin/low-spin crossover [12,24]. Long-range magnetic ordering can be indexed on a $\sqrt{2}a \times \sqrt{2}a \times c$ expansion of the nuclear cell with moment orientations and a magnitude in line with previously reported closely related analogues. The spectrum of spin-states for related materials containing Ni^{2+} ions in highly elongated environments is shown in Fig. 9 with the crossover as a function of Ni–O bond length depicted.

Credit authors statement

Robert D. Smyth: Wrote the paper along with input from YT and SJC. **Dmitry Khalyavin:** Collected the data which was analysed by RDS.

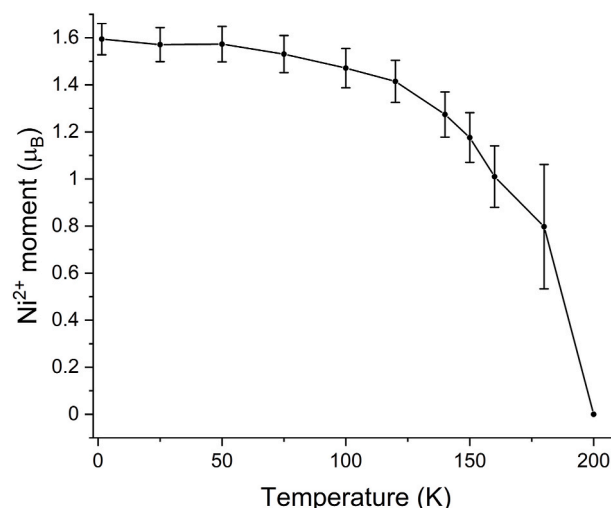


Fig. 8. Thermal evolution of the ordered Ni^{2+} moment in $\text{Sr}_2\text{NiO}_2\text{Cl}_2$. The moment at 200 K has been fixed at 0 as a guide to the eye as there was no evidence for any remaining magnetic intensity at that temperature.

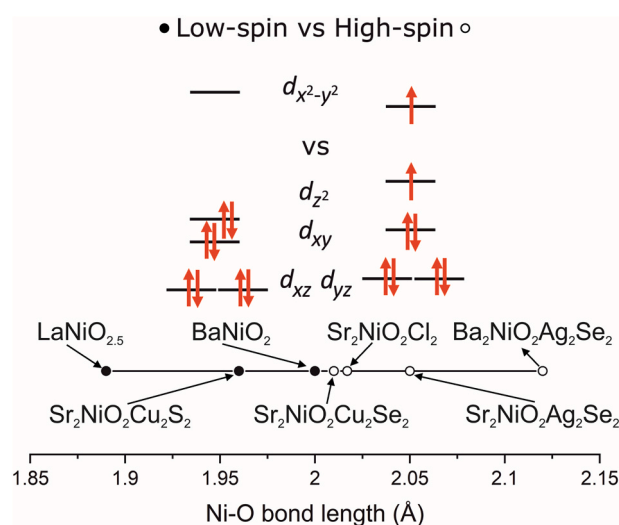


Fig. 9. Ni–O bond length comparison and the spin-state for various Ni^{2+} containing solids [1,12,25–27]. [12,25–27].

Yoshihiro Tsujimoto and Kazunari Yamaura: Synthesised the sample. **Simon J. Clarke:** Contributed to the discussion of the results and provided the research framework.

Declaration of competing interest

The authors declare no conflicts of interest that could inappropriately influence, or be perceived to influence, our work.

Data availability

Data will be made available on request.

Acknowledgements

We would like to thank the UK EPSRC (EP/T027991/1, EP/R513295/1 and EP/R042594/1) and JSPS Core-to-Core Program (JPJSCCA20200004) for funding and for studentship support for R.D.S. We thank the ISIS pulsed and muon source (RB2200301) and Diamond Light Source (DLS) Ltd (CY25166 and CY32893) for the award of beam

time. We thank Dr L. Saunders and Dr C. Murray for support on I11 (DLS). Y.T. acknowledges the grant from the Murata Science Foundation. K.Y. acknowledges the grant from the Kazuchika Okura Memorial Foundation.

Appendix A. Supplementary data

Supplementary data to this article can be found online at <https://doi.org/10.1016/j.solidstatesciences.2023.107297>.

References

- [1] S.J. Clarke, P. Adamson, S.J.C. Herkelrath, O.J. Rutt, D.R. Parker, M.J. Pitcher, C. F. Smura, Structures, physical properties, and chemistry of layered oxychalcogenides and oxypnictides, *Inorg. Chem.* 47 (2008) 8473–8486, <https://doi.org/10.1021/ic8009964>.
- [2] H. Kageyama, K. Hayashi, K. Maeda, J.P. Attfield, Z. Hiroi, J.M. Rondinelli, K. R. Poeppelmeier, Expanding frontiers in materials chemistry and physics with multiple anions, *Nat. Commun.* 772 (2018), <https://doi.org/10.1038/s41467-018-02838-4>.
- [3] R. Marchand, Y. Laurent, J. Guyader, P. L'Haridon, P. Verdier, Nitrides and oxynitrides: preparation, crystal chemistry and properties, *J. Eur. Ceram. Soc.* 8 (1991) 197–213, [https://doi.org/10.1016/0955-2219\(91\)90096-I](https://doi.org/10.1016/0955-2219(91)90096-I).
- [4] D.L. Sidebottom, M.A. Hruschka, B.G. Potter, R.K. Brow, Structure and optical properties of rare earth-doped zinc oxyhalide tellurite glasses, *J. Non-Cryst. Solids* 222 (1997) 282–289, [https://doi.org/10.1016/S0022-3093\(97\)90125-3](https://doi.org/10.1016/S0022-3093(97)90125-3).
- [5] S.D.N. Luu, P. Vaqueiro, Layered oxychalcogenides: structural chemistry and thermoelectric properties, *J. Mater. Chem.* 131–140 (2016), <https://doi.org/10.1016/j.jmat.2016.04.002>.
- [6] Y. Kamihara, T. Watanabe, M. Hirano, H. Hosono, Iron based layered superconductor $\text{La}[\text{O}_{1-x}\text{F}_x]\text{FeAs}$ ($x = 0.05 - 0.12$) with $T_c = 26$ K, *J. Am. Chem. Soc.* 130 (2008) 41, <https://doi.org/10.1021/ja800073m>.
- [7] R. Pastrana-Fábregas, J. Isasi-Marín, R. Sáez-Puche, Synthesis and characterization of inorganic pigments based on transition metal oxynitrides, *J. Mater. Res.* 21 (2006) 2255–2260, <https://doi.org/10.1557/jmr.2006.0272>.
- [8] D. Vaknin, S.K. Sinha, C. Stassis, L.L. Miller, D.C. Johnston, Antiferromagnetism in $\text{Sr}_2\text{CuO}_2\text{Cl}_2$, *Phys. Rev. B* 41 (1990) 1926–1933, <https://doi.org/10.1103/PhysRevB.41.1926>.
- [9] E. Dixon, M.A. Hayward, The topotactic reduction of $\text{Sr}_3\text{Fe}_2\text{O}_5\text{Cl}_2$ square planar Fe (II) in an extended oxyhalide, *Inorg. Chem.* 49 (2010) 9649–9654, <https://doi.org/10.1021/ic101371z>.
- [10] G. Hyett, N. Barrier, S.J. Clarke, J. Hadernmann, Topotactic oxidative and reductive control of the structures and properties of layered manganese oxychalcogenides, *J. Am. Chem. Soc.* 129 (2007) 11192–11201, <https://doi.org/10.1021/ja073048m>.
- [11] J.N. Blandy, D.R. Parker, S.J. Cassidy, D.N. Woodruff, X. Xu, S.J. Clarke, Synthesis, structure, and compositional tuning of the layered oxide tellurides $\text{Sr}_2\text{MnO}_2\text{Cu}_2\text{Te}_2$ and $\text{Sr}_2\text{CoO}_2\text{Cu}_2\text{Te}_2$, *Inorg. Chem.* 58 (2019) 8140–8150, <https://doi.org/10.1021/acs.inorgchem.9b00919>.
- [12] R.D. Smyth, J.N. Blandy, Z. Yu, S. Liu, C.V. Topping, S.J. Cassidy, C.F. Smura, D. N. Woodruff, P. Manuel, C.L. Bull, N.P. Funnell, C.J. Ridley, J.E. McGrady, S. J. Clarke, High- versus low-spin Ni^{2+} in elongated octahedral environments: $\text{Sr}_2\text{NiO}_2\text{Cu}_2\text{Se}_2$, $\text{Sr}_2\text{NiO}_2\text{Cu}_2\text{S}_2$, and $\text{Sr}_2\text{NiO}_2\text{Cu}_2(\text{Se}_{1-x}\text{S}_x)_2$, *Chem. Mater.* 34 (2022) 9503–9516, <https://doi.org/10.1021/acs.chemmater.2c02002>.
- [13] Y. Tsujimoto, C.I. Sathish, Y. Matsushita, K. Yamaura, T. Uchikoshi, New members of layered oxychloride perovskites with square planar coordination: $\text{Sr}_2\text{MO}_2\text{Cl}_2$ ($M = \text{Mn}, \text{Ni}$) and $\text{Ba}_2\text{PdO}_2\text{Cl}_2$, *Chem. Commun.* 50 (2014) 5915–5918, <https://doi.org/10.1039/c4cc01422g>.
- [14] W. Zhou, S. Li, S. Wu, Magnetic and electronic properties of layered $\text{Sr}_2\text{NiO}_2\text{Cl}_2$ with square planar coordination, *J. Magn. Magn. Mater.* 514 (2020), 167195, <https://doi.org/10.1016/j.jmmm.2020.167195>.
- [15] S. Ueda, Y. Katsuya, M. Tanaka, H. Yoshikawa, Y. Yamashita, S. Ishimaru, Y. Matsushita, K. Kobayashi, Present status of the NIMS contract beamline BL15XU at SPring-8, *AIP Conf. Proc.* 1234 (2010) 403–406, <https://doi.org/10.1063/1.3463225>.
- [16] S.P. Thompson, J.E. Parker, J. Potter, T.P. Hill, A. Birt, T.M. Cobb, F. Yuan, C. C. Tang, Beamline I11 at Diamond: a new instrument for high resolution powder diffraction, *Rev. Sci. Instrum.* 80 (2009), 075107, <https://doi.org/10.1063/1.3167217>.
- [17] L.C. Chapon, P. Manuel, P.G. Radaelli, C. Benson, L. Perrott, S. Ansell, N.J. Rhodes, D. Raspino, D. Duxbury, E. Spill, J. Norris, WISH The New Powder and Single Crystal Magnetic Diffractometer on the Second Target Station, *Neutron News* p 22–25, (2011), <https://doi.org/10.1080/10448632.2011.569650>.
- [18] K. Momma, F. Izumi, VESTA 3 for three-dimensional visualization of crystal, volumetric and morphology data, *J. Appl. Crystallogr.* 44 (2011) 1272–1276, <https://doi.org/10.1107/S0021889811038970>.
- [19] J.N. Blandy, S. Liu, C.F. Smura, S.J. Cassidy, D.N. Woodruff, J.E. McGrady, S. J. Clarke, Synthesis, structure, and properties of the layered oxide chalcogenides $\text{Sr}_2\text{CuO}_2\text{Cu}_2\text{S}_2$ and $\text{Sr}_2\text{CuO}_2\text{Cu}_2\text{Se}_2$, *Inorg. Chem.* 57 (2018) 15379–15388, <https://doi.org/10.1021/acs.inorgchem.8b02698>.
- [20] W.L. Roth, Magnetic structures of MnO , FeO , CoO , and NiO , *Phys. Rev.* 110 (1958) 1333–1341, <https://doi.org/10.1103/PhysRev.110.1333>.
- [21] B.J. Campbell, H.T. Stokes, D.E. Tanner, D.M. Hatch, ISODISPLACE: a web-based tool for exploring structural distortions, *J. Appl. Crystallogr.* 39 (2006) 607–614, <https://doi.org/10.1107/S0021889806014075>.
- [22] A.A. Coelho, TOPAS and TOPAS-academic: an optimization Program integrating computer algebra and crystallographic objects written in C++, *J. Appl. Crystallogr.* 51 (2018) 210–218 (Version 6).
- [23] D.B. Litvin, Magnetic group tables: 1-, 2- and 3-dimensional magnetic subperiodic groups and magnetic space groups, *Int. Union Crystallogr.* (2013), <https://doi.org/10.1107/9780955360220001>.
- [24] R.D. Shannon, Revised effective ionic radii and systematic studies of interatomic distances in halides and chalcogenides, *Acta Crystallogr., Sect. A* 32 (1976) 751–767, <https://doi.org/10.1107/S0567739476001551>.
- [25] J.A. Alonso, M.J. Martínez-Lope, J.L. García-Muñoz, M.T. Fernández, Crystal structure and magnetism in the defect perovskite $\text{LaNiO}_{2.5}$, *Phys. B Condens. Matter* 234–236 (1997) 18–19, [https://doi.org/10.1016/S0921-4526\(96\)00863-0](https://doi.org/10.1016/S0921-4526(96)00863-0).
- [26] M. Matsuda, K. Katsumata, A. Zheludev, S.M. Shapiro, G. Shirane, Neutron scattering study in BaNiO_2 , *J. Phys. Chem. Solid.* 60 (1999) 1121–1123, [https://doi.org/10.1016/S0022-3697\(99\)00070-0](https://doi.org/10.1016/S0022-3697(99)00070-0).
- [27] Y. Matsumoto, T. Yamamoto, K. Nakano, H. Takatsu, T. Murakami, K. Hongo, R. Maezono, H. Ogino, D. Song, C.M. Brown, C. Tassel, H. Kageyama, High-pressure synthesis of $\text{A}_2\text{NiO}_2\text{Ag}_2\text{Se}_2$ ($A = \text{Sr}, \text{Ba}$) with a high-spin Ni^{2+} in square-planar coordination, *Angew. Chem. - Int. Ed.* 58 (2019) 756–759, <https://doi.org/10.1002/anie.201810161>.